Catalysis Communications 187 (2024) 106850

Contents lists available at ScienceDirect

Catalysis Communications

journal homepage: www.elsevier.com/locate/catcom

H_2 production by solar photoreforming of plastic materials using SiC-g-C_3N_4composites

Maria Teresa Armeli Iapichino [a], Roberto Fiorenza [a,*], Vincenzo Patamia [b], Giuseppe Floresta [b], Antonino Gulino [a,c], Marcello Condorelli [a], Giuliana Impellizzeri [d], Giuseppe Compagnini [a], Salvatore Sciré [a]

[a] Department of Chemical Sciences, University of Catania, V.le A. Doria 6, 95125 Catania, Italy
[b] Department of Drug and Health Sciences, University of Catania, V.le A. Doria 6, 95125 Catania, Italy
[c] INSTM UdR of Catania, V.le A. Doria 6, 95125 Catania, Italy
[d] CNR-IMM, Via S. Sofia 64, 95123 Catania, Italy

ARTICLE INFO

Keywords:
H_2
PET
BPA
SiC
C_3N_4
Solar photoreforming

ABSTRACT

The photoreforming of polyethylene terephthalate and bisphenol A was here investigated using uncommon photocatalysts (SiC-g-C_3N_4 composites). The results showed as the addition of small amounts of g-C_3N_4 on SiC promoted an efficient charge carriers separation and a good interaction between the two materials, leading to a H_2 production rate of 18 and 12 $\mu molH_2/g_{cat}$•h for the photoreforming of polyethylene terephthalate and bisphenol A, respectively. The accurate selection of different g-C_3N_4 precursors, combined with the appropriate control of the key reaction parameters (pH and plastic materials pretreatments) allowed to optimize the performance of the SiC-g-C_3N_4 composites for the photocatalytic H_2 production.

1. Introduction

The ever-increasing consumption of fossil fuels over the years, has caused significant damage to the environment such as global warming and depletion of energy resources [1]. Consequently, nowadays there is a growing interest in the development of clean and sustainable processes. One of the possible strategies to favour the energy decarbonization with green methodologies is the use of hydrogen because this energy vector can create synergies between the exploitation of the renewable energy resources and the environment protection.

The most widespread methodology for the hydrogen production is the steam reforming of non-renewable fossil hydrocarbons. Hence, the 48% of H_2 production comes from the reforming of natural gas, 30% from the reforming of oil, and 18% from the reforming of coal [2]. Lastly, 4% of hydrogen is produced by water electrolysis. Currently the annual production of hydrogen is about 0.1 GT which is consumed mainly on site in refining and processing of metals, and at small extent as fuel in fuel cells [2]. Today, the most important limitation of the sustainable (green) hydrogen production, i.e., H_2 obtained from renewables, is its higher cost compared to the standard fossil fuels-based processes (grey or black hydrogen). The use of the sun, as energy driving force, could help to decrease the price. Another fascinating and green way to obtain hydrogen is the photocatalysis, mainly through the photoreforming process that allowed to increase the H_2 generation compared to the overall photocatalytic water splitting [3,4]. Indeed, the simple reaction of the water splitting ($2H_2O \rightarrow 2H_2 + O_2$), is not effective from the energy point of view [3]. The solar photoreforming process (PR) combines the water reduction with the oxidation of an organic sacrificial agent on a semiconductor material. In a typical process the electrons in the photocatalyst are excited by sunlight to the conduction band (CB) reducing the protons of the H_2O to H_2. Consequently, the holes generate in the photocatalyst valence band (VB) oxidize the organic substrate ($C_xH_yO_z$) to CO_2 or to intermediate products with a further H_2 evolution: $C_xH_yO_z + (2x - z)H_2O \rightarrow^{h\nu} \left(2x - z - \frac{y}{2}\right)H_2 + x\,CO_2$ [5–7].

In this way the organic compound has the function of holes scavenger that delays the recombination between the excited electrons and the holes, a common reason of the photocatalyst deactivation, allowing to increase the H_2 formation. To favour the PR reaction, the incident photons should be higher or equal in energy than the semiconductor band gap, the CB of the semiconductor should be more negative than the reduction potential of H^+ to H_2 (−0.41 V vs. the reversible hydrogen electrode (RHE) at pH = 7), and VB should be more positive than the

* Corresponding author.
E-mail address: rfiorenza@unict.it (R. Fiorenza).

https://doi.org/10.1016/j.catcom.2024.106850
Received 5 December 2023; Received in revised form 11 January 2024; Accepted 16 January 2024
Available online 17 January 2024

oxidation potential of H_2O/O_2 (0.82 V at pH = 7) and of the organic compound to a given oxidation product (depending on the specific holes scavenger used) [4].

Due to the high versatility of the PR reaction, in this work we have investigated the use of plastic-related materials as sacrificial agents for the PR, in order to encompass two distinct questions (the water pollution by the plastic materials and the production of H_2) with a single process. This is a novel approach, which allows to convert plastic pollutants and to obtain hydrogen. Plastics are fundamentals for nowadays, and are applied in various areas, including security food health and agriculture. However, about 8 million tons of plastics enter into the ocean, therefore the unrecyclable plastics present environmental problems and a huge loss of material value [8]. In particular, the production of polyethylene terephthalate (PET) is ~30 million tons, (globally used in textiles and packaging including bottles), but only 9% of PET is recycled [9]. A large amount of consumed plastics causes the "white pollution" because plastics are not degraded naturally or the time of degradation is in the order of centuries. In this contest the photocatalytic process can be a suitable solution for this problem [10].

For these reasons in this work, we used the PET from commercial bottles as organic compound for the solar photoreforming. Moreover, the Bisphenol A (BPA), a largely used monomer for the production of polycarbonate and flame-retardant epoxy resins, not easily removed from wastewaters with the biological or the standard treatments [11–13], was also investigated as sacrificial agent of PR reaction.

Another key point is the proper choice of the photocatalyst for the photoreforming. The most employed and investigated photocatalyst, until now, is the titanium dioxide [14]. Over the years, the European Commission provided a critical assessment of the most used raw materials, taking into account the economic importance and the supply risk. In the 2020 the titanium metal entered in this list, and this was also confirmed in the updated 2023 list [15]. For this reason, it is necessary to search new alternatives and not-critical materials also for photocatalytic applications in order to increase the overall sustainability of the processes. This study focuses on the performance of composites made by silicon carbide (SiC) and graphitic carbon nitride (g-C_3N_4). The combination of these materials and the photocatalytic performance of the obtained composites are not fully explored in the literature.

SiC was largely used in catalysis especially as support due to its high thermal and chemical stability in both acidic and basic conditions [16]. Furthermore, for its tuneable bandgap (2.4–3.3 eV) and for its high charge-carriers mobility, was recently investigated in form of different nanostructures, for several photocatalytic applications under ultraviolet-visible light radiation [17].

Similarly, the band gap of g-C_3N_4 (about 2.8–2.9 eV) and the energy levels of its valence and conduction band are sufficiently large to overcome the thermodynamic requirement of the water splitting and the photoreforming reactions [18]. Moreover, the carbon nitride possesses the advantages of low cost, low toxicity, thermodynamic stability, and remarkable optical properties [19]. It can be easily prepared with the thermodegradation of green precursors [20] and its 2D structure can facilitate the electrons mobility, increasing the charge carriers separation in the composite materials [21].

At the best of our knowledge, this is the first time that SiC-g-C_3N_4 composites prepared with a green and simple procedure have been tested for the solar photoreforming of plastic materials, in order to find fascinating and innovative solutions for the H_2 production improving at the same time the overall sustainability of the process (including the employed materials). This will allow to propose new strategies to obtain H_2 from water contaminants.

2. Experimental

2.1. Materials preparation

The SiC-g-C_3N_4 composites were prepared mixing the commercial silicon carbide powder (Sigma Aldrich, MKCN0364 357,391, β-SiC) with diverse amounts of urea (Fluka, BioChemika ≥99.5%) to obtain different composites with various weight percentages of carbon nitride. Indeed, one of the easy and green reported methodology for the preparation of the g-C_3N_4 is the urea thermodegradation [22]. Specifically, the SiC and the urea powders were put in a covered alumina crucible and heated in a muffle at 450 °C with a ramp of 5 °C/min for 5 h. For the photocatalytic comparison also the bare SiC was treated under the same thermal conditions of the SiC-g-C_3N_4 composites.

2.2. Samples characterization

X-ray powder diffraction (XRD) measurements were performed with a PANalytical X'pertPro X-ray diffractometer using a Cu Kα radiation. The obtained diffraction peaks were matched with those present in the JCPDS Data File.

The UV–Vis DRS (Diffuse Reflectance Spectroscopy) was carried out with a JASCO V-670 spectrophotometer The E_g (optical band gap) of the samples was estimated by plotting the modified Kubelka–Munk function versus the hν [23].

The TEM images were acquired with a JEOL JEM 1400 microscope. The catalysts were dispersed in 2-propanol and sonicated for 30 min. After this treatment they were deposited onto copper grids.

X-ray photoelectron spectra (XPS) were acquired at 45° take-off angle relative to the surface sample holder, with a PHI 5000 Versa Probe II system (ULVAC-PHI, INC., base pressure of the main chamber 1 × 10^{-8} Pa). The powders were excited with the monochromatized Al Kα X-ray radiation with a pass energy of 5.85 eV. The instrumental energy resolution was ≤0.5 eV. The XPS peak intensities were obtained after Shirley background removal. Spectra calibration was achieved by fixing the Ag $3d_{5/2}$ peak of a clean sample at 368.3 eV [24]; this method turned the C1s peak of the adventitious carbon contamination at 285.0 eV [24,25].

Photoluminescence (PL) spectra were obtained with a Horiba JobinYvon spectrofluorometer. It was used a λ of excitation of 350 nm.

Zeta potential measurements were performed with a HORIBA analyser SZ-100 in disposable PMMA cuvettes with graphite electrode, applying a 3 mV potential.

The textural properties of the samples were determined by the N_2 adsorption-desorption measurements at −196 °C with a Micromeritics Tristar II Plus 3020 instrument. The samples were pretreated outgassing at 100 °C overnight.

2.3. Photocatalytic setup

For the photocatalytic hydrogen production, a home-made Pyrex jacketed reactor thermostated at 30 °C was used, following the experimental procedures reported in the ref. [26]. The photocatalytic tests were performed with 50 mg of the photocatalyst, homogeneously suspended in an aqueous solution containing the sacrificial agent (40 mL of deionized water and 10 mL of BPA or PET solution) inside the reactor. Then the reactor was irradiated for 5 h using a special solar lamp (Osram Ultra Vitalux 300 W, irradiance of 10.7 mW/cm^2). BPA (Sigma Aldrich 98%) and PET (from a commercial bottle) were pre-treated in order to obtain a solution of the sacrificial agent [27]. In particular, 50 mg of BPA was solubilized in a 10 M NaOH solution, whereas 50 mg of PET (the PET bottle was previously crushed and transformed in powders of 140–70 mesh) were solubilized in 10 M NaOH solution kept under stirring for 6 days at 40 °C. The measurements were replied three times (3% error).

The byproducts detection of the BPA and PET photoreforming was performed by ^{1}H-NMR. The ^{1}H -NMR spectra were recorded at 300 K on a Varian UNITY Inova using D_2O as the solvent at 500 MHz. 128 scans were performed for each sample. The water signal suppression was obtained by applying the PRESAT (WATER) pulse sequence, and the ^{1}H-NMR (PRESAT) optimized acquisition parameters were as follows:

relaxation delay (1 s), 128 scans and spectral width from 0 to 11 ppm [28].

3. Results and discussion

3.1. Solar photoreforming of BPA

The Fig. 1 illustrates the H_2 production rate obtained by the solar photoreforming of BPA. In these tests the influence of the addition of different amounts of SiC to g-C_3N_4 and the photocatalytic activity both of SiC-g-C_3N_4 and g-C_3N_4-SiC composites were evaluated.

From the reported data it is clear as the SiC-based samples gave the best H_2 production rate whereas the inverse g-C_3N_4-based composites (g-C_3N_4-SiC) gave a negligible evolution of H_2. In accordance with the literature, indeed, due to the high charge carriers recombination of carbon nitride, the photocatalytic features were better exploited when g-C_3N_4 is used as co-catalyst or as minor component of a composite and not as the main one [29,30]. The addition of small amount of g-C_3N_4 increased the production of H_2 from 6 μmol/g_{cat}•h of the bare SiC to 12 μmol/g_{cat}•h of the SiC-0.5%g-C_3N_4 composite. It is important to highlight that the SiC sample underwent the same thermal treatment of the SiC-based composites, i.e., calcination at 450 °C for 5 h, and that the untreated SiC sample (as purchased) gave a slight lower H_2 production (5 μmol/g_{cat}•h, data not showed). A higher amount of carbon nitride on SiC had a detrimental effect with a lower H_2 production, probably because an excess of carbon nitride led to the coverage of the surface-active sites of SiC. The pretreatments of BPA (50 mg solubilized in NaOH 10 M) led to a highly basic pH (13) of the reactant solution. Consequently, the influence of the pH on the photocatalytic activity was investigated using the best photocatalyst (SiC-0.5%g-C_3N_4) and the results are reported in the Fig. 2A. Interestingly, basic pH (pH = 13) is necessary to both guarantee a good H_2 production with an efficient BPA solubilization/photo-oxidation. Indeed, if the test was carried out at pH = 7 (through neutralization of the BPA basic solution with a solution of HNO_3 10 M) the H_2 production rate drastically decreased up to 1 μmol/g_{cat}•h, whereas acidic conditions (50 mg of BPA solubilized in a solution of HNO_3 10 M) unfavoured the H_2 evolution. Probably the presence of a high number of OH^- species in the basic environment boosted up the BPA photo-oxidation with a consequent increase of the H_2 production.

In this contest Fig. 2B compares the H_2 production rates obtained with the SiC-0.5%g-C_3N_4 composite in the overall water splitting test (i.e., without addition of BPA, pure demineralized water, pH = 7) and in water + NaOH solution (40 mL of water +10 mL of NaOH 10 M, pH = 13). The overall water splitting did not allow to obtain significant H_2 amount, pointing to as the presence of a sacrificial agent, as the BPA, is necessary for the H_2 formation. The H_2 production rate of the solution containing only water and NaOH solution was also low (1 μmol/g_{cat}•h), thus suggesting that the OH^- ions gave a substantial contribution to the H_2 evolution only with the contextual presence of BPA. Indeed, the hydroxyl species can improve the photo-oxidation of BPA, that acting as holes scavenger, allowed to increase the e^-/h^+ separation on the SiC-0.5%g-C_3N_4 composite [31]. As a result, the solar H_2 evolution increased in the BPA photoreforming test up to 12 μmol/g_{cat}•h.

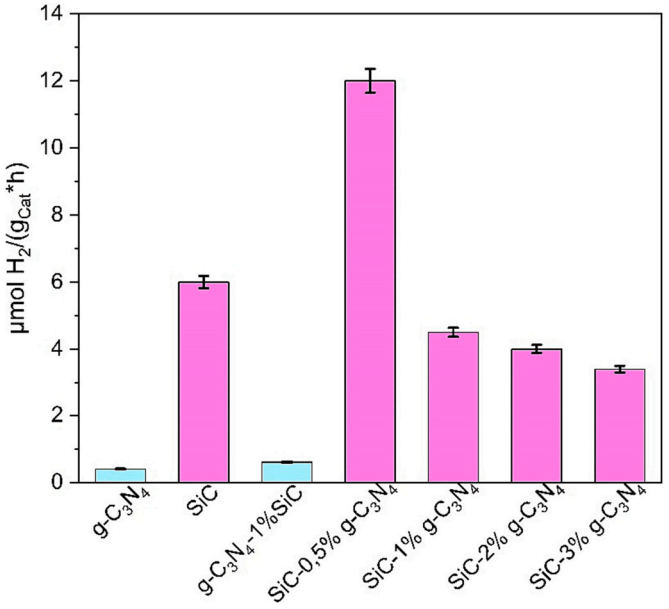

Fig. 1. H_2 production rates for the SiC and the g-C_3N_4-based samples.

To get more insight in the mechanism of the BPA photo-oxidation, ^{1}HNMR spectra were carried out before and after the photoreforming reaction using the SiC-0.5%g-C_3N_4 composite (Fig. S1). Before the reaction it is possible to note the signals related to the aliphatic CH_3 (0.8 ppm) and aromatic protons of BPA (5.78 and 6.29 ppm). After the photoreforming the disappearance of these signals was verified and, in accordance with the literature, the formation of small molecules such as acetaldehyde hydrate (signals at 2.21 and 6.21 ppm) was observed [32]. These small molecules were more reactive towards the photoreforming, allowing to increase the H_2 evolution [33].

In summary, with the best composite (SiC-0.5%g-C_3N_4) and at basic pH, a good BPA photocatalytic degradation was guaranteed with the formation of small organic compounds that boosted the H_2 formation by the contextual photoreforming of both BPA and these intermediate products.

3.2. Solar photoreforming of PET

Fig. 3 depicts the comparison among the various investigated samples in the photoreforming of PET and BPA. It is possible to note as the PET photoreforming allowed to obtain a higher H_2 production rate compared to the BPA, with the best composite, in this case the SiC-1%g-C_3N_4, that led to 18 μmolH_2/g_{cat}•h after 5 h of solar PET photoreforming. Due to the employed PET pretreatment also in this case the pH of the reaction mixture was 13. It is important to highlight that a lower amount of 0.5 wt% of g-C_3N_4 was not sufficient to establish a good interaction with SiC, being the H_2 production similar or only slightly higher compared to the bare SiC for both BPA and PET photoreforming (Fig. 3).

As reported in the literature [34] the higher H_2 evolution of PET photoreforming compared to the BPA can be related to the byproducts formed during the reaction. Indeed, the ethylene glycol (EG) was the main intermediate formed during the PET photoreforming and its formation was favoured by the hydrolysis under basic conditions [35].The formation of EG was beneficial for the H_2 production by photoreforming due to its tendency to fully decompose into H_2 and CO_2 under mild condition and UV/solar irradiation in the presence of several photocatalysts [9]. The formation of EG was verified by ^{1}HNMR using the SiC-1% g-C_3N_4 sample (Fig. S2). The spectrum of the pre-treated PET before the photoreforming showed signals related to ethylene glycol (2.92 ppm) and terephthalate (7.30 ppm). After the reaction it is possible to note the complete disappearance of these signals and the formation of new peaks attributable to different degradation products such as formate (7.74 ppm) or small carboxylic acids (3.50 ppm) [36].

Being the PET photoreforming more efficient than the BPA photoreforming, we tested the influence of the different carbon nitride precursors (urea, thiourea and melamine) to obtain the SiC-g-C_3N_4 photocatalysts (Fig. 4). Although in the literature the melamine was the most used precursors for the synthesis of the g-C_3N_4-based materials [37–39], in our experimental conditions the use of urea led to the best interaction of the formed carbon nitride and the SiC. Consequently, the SiC-g-C_3N_4 samples prepared using urea as carbon nitride precursor gave the best performance in the PET photoreforming. Probably, in the case of thiourea, the formation of sulphur-based impurities during the

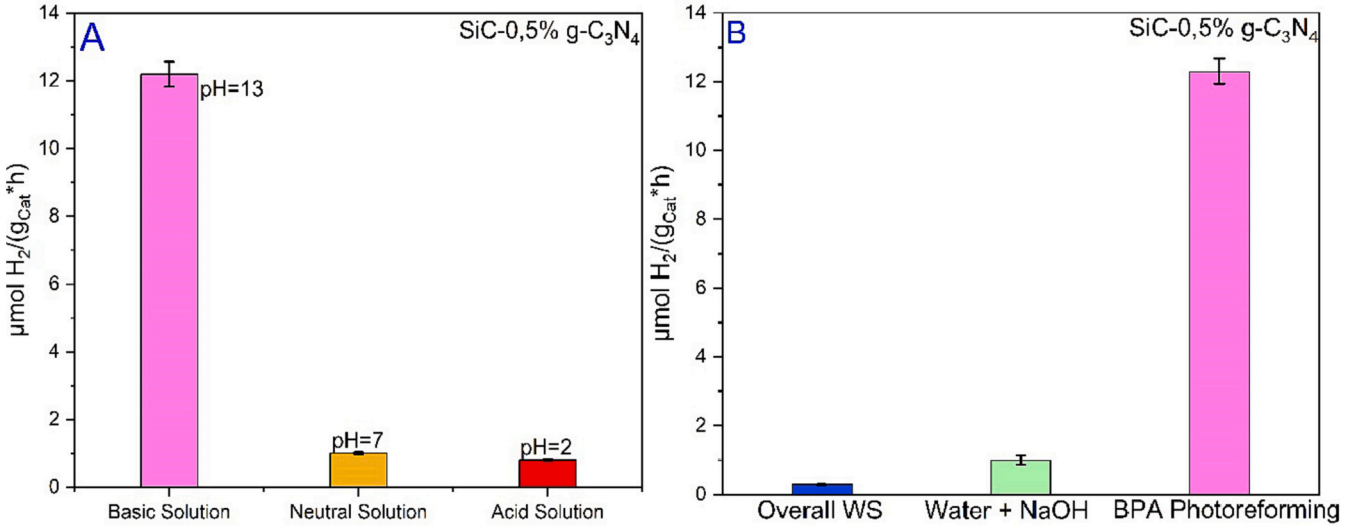

Fig. 2. (A) Influence of the pH on the BPA photoreforming using the SiC-0,5% g-C_3N_4 sample, (B) comparison among the H_2 production rates of the overall water splitting, the water splitting+NaOH and the BPA photoreforming.

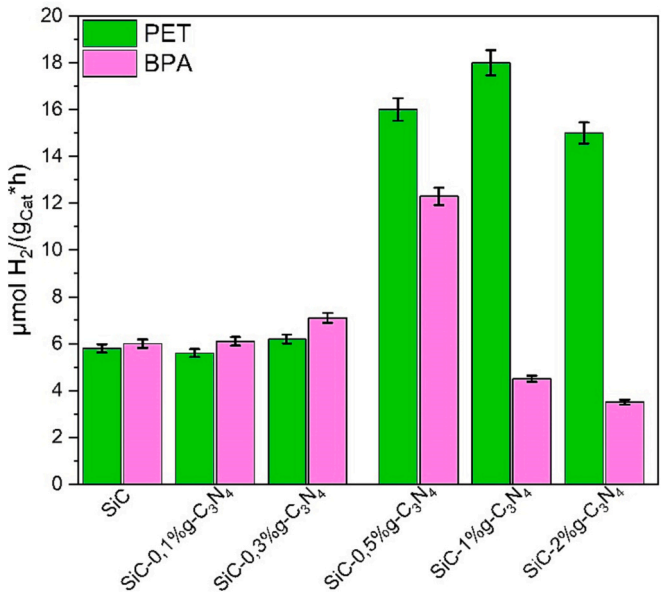

Fig. 3. H_2 production rates of the photoreforming of PET and BPA using the SiC-g-C_3N_4-based samples.

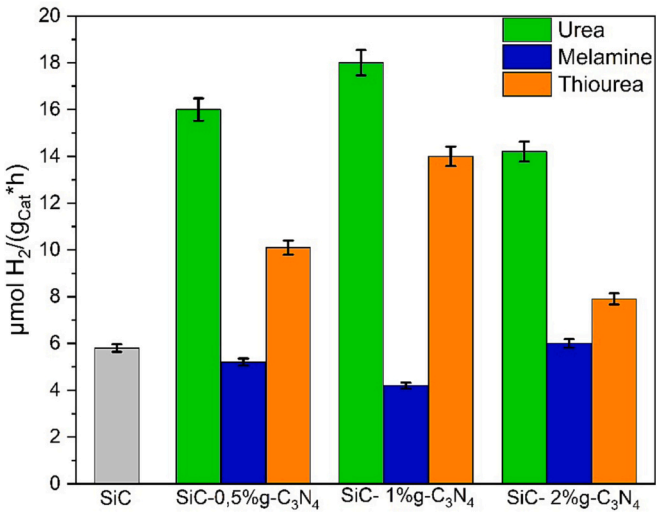

Fig. 4. H_2 production rates for the PET photoreforming using several SiC-g-C_3N_4-based composites prepared with different carbon nitride precursors.

thermodegradation process affected the photoactivity of the composite [40], whereas in the case of melamine the eventual presence of contaminants or a not complete amine groups condensation [41] significantly affect the performance of the SiC-based composites. Indeed, the H_2 production rates of the SiC-based photocatalysts prepared using melamine were lower compared also to the bare SiC (Fig. 4), whereas the samples synthetized from thiourea gave worse results compared to the same ones prepared with urea. It is important to note that on the basis of the literature data, to favour the carbon nitride precursors thermodegradation, the composites synthesized starting from thiourea were treated at 500 °C for 5 h (heating ramp of 5 °C/min), whereas the samples prepared from melamine at 550 °C for 5 h with the same heating ramp [42,43]. These higher thermal treatments compared to the procedures used for the composites prepared starting from urea (heated at 450 °C for 5 h with a ramp of 5 °C/min) can induce the agglomeration of the SiC particles, modifying its structural properties and then the interaction with the in-situ formed g-C_3N_4. As consequence, the H_2 production of the composites synthesized from thiourea, and melamine was lower compared to that of analogous samples prepared with urea as g-C_3N_4 precursor. Furthermore, it was recently demonstrated that the use of urea allowed to obtain the ideal C/N molar ratio (0.75) with smaller thickness of the g-C_3N_4 sheets compared to other precursors [41,44,45].

The influence of the pH was also investigated in the PET photoreforming on the best composite (in this case the SiC-1%g-C_3N_4 prepared from urea), and the results are shown in Fig. 5A. Similarly, to the BPA photoreforming, strong basic pH was fundamental to both guarantee good H_2 production and PET solubilization/photo-oxidation, whereas the neutralization with 10 M HNO_3 solution or acidic conditions (PET pretreatment in a 10 M HNO_3 solution) led to a drastic decrease of the photoactivity of the SiC-1%g-C_3N_4 composite.

Considering also the results obtained in the BPA photoreforming, these data pointed to the importance of the basic environment for the surface charge of the SiC-based samples and the corresponding adsorption of the reaction mixture. In this contest, the Zeta potential on the SiC-1%g-C_3N_4 photocatalyst was measured (Fig. 5B). The sample showed a negative surface charge independently of the pH. However, at

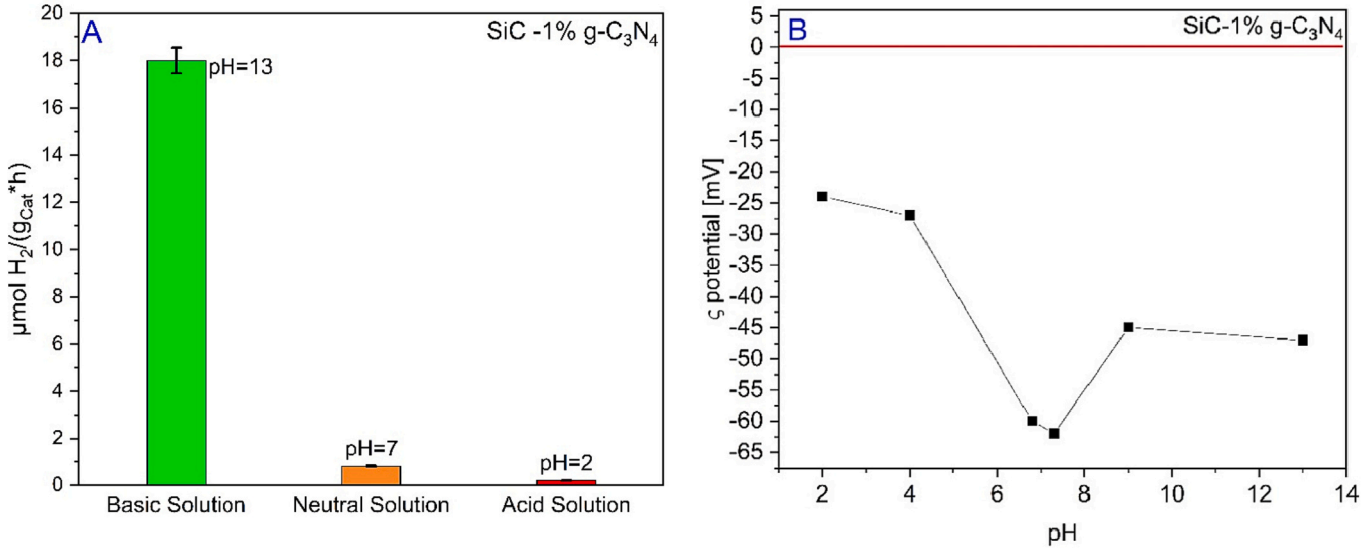

Fig. 5. (A) Influence of the pH on the PET photoreforming using the SiC -1% g-C_3N_4 sample, (B) *Z*-potential of the SiC 1% g-C_3N_4 composite.

the best condition for both the BPA and PET photoreforming (pH = 13) the potential had an intermediate negative value (−46 mV) compared to neutral pH (the most negative value, −63 mV) and to acidic pH (the least negative value, −24 mV at pH = 2). Reasonably, strong basic pH favours a balance between different factors, as the BPA and the PET degradation favoured by the formation of the ideal amount of OH^- ions, that allowed also an efficient interaction between the generated H^+ and the surface negative charge of the SiC-1%g-C_3N_4 photocatalyst. Indeed, it is worth to note that, from a preliminary photocatalytic screening (data not shown), using a more diluted NaOH solution (pH < 13) a strong drop down of the photocatalyst performance was verified with negligible H_2 formation, confirming the importance of a strong basic environment both for PET and BPA photoreforming.

3.3. Correlation between the photocatalytic activity and the composite characterization

The optical properties of the samples were determined by UV-DRS (Fig. S3) and PL spectroscopies (Fig. 6). The estimation of the optical band gap (E_g) was carried out by the modified Kubelka-Munk function [23] and the results are reported in the Table 1, together with the textural properties measured by the N_2-adsorption-desorption measurements.

There are no substantial variations in the E_g values of the SiC-based composites that exhibited a slightly higher E_g compared to the bare g-C_3N_4. The BET surface area values were in accordance with the literature data concerning the as-purchased SiC (in the β form) and the bare g-C_3N_4 prepared from urea [46,47].The addition of a growing amount of carbon nitride on SiC led to a slight increase of the surface area (from 17 m^2/g of the bare SiC to 23 m^2/g of the SiC 2% g-C_3N_4) with a consequent decrease of the mean pores diameter and the pores volume (Table 1). However, these slight variations did not affect significantly the photocatalytic performance in the examined photoreforming reactions, being the composites with low amounts of g-C_3N_4 the most active ones (SiC 0,5% g-C_3N_4 for the BPA photoreforming, SiC 1% g-C_3N_4 for the PET photoreforming).

The PL spectroscopy was carried out to elucidate the possible

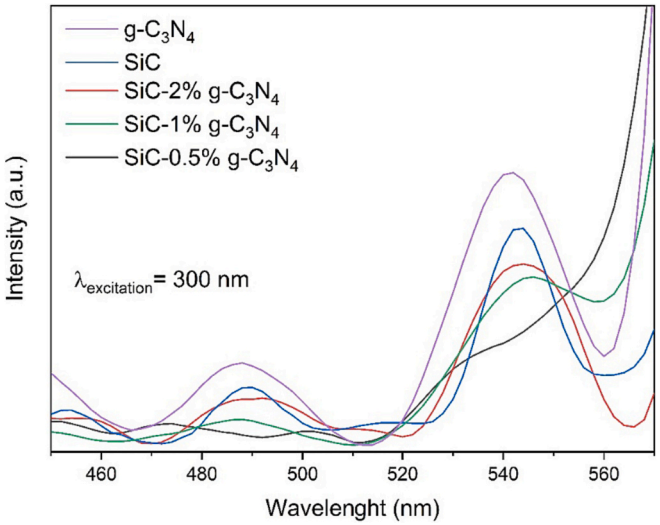

Fig. 6. Photoluminescence spectra of the analysed composites.

electron transfer and the separation efficiency of the photogenerated charge carriers in the as-prepared samples [48,49]. Generally, a relatively weak PL bands intensity is correlated to a low recombination rate in the semiconductors [50]. From the Fig. 6 it is possible to note that all samples showed two bands centred at about 487 and 542 nm, usually associated to the excitation/recombination phenomena of the charge carriers of SiC-based materials [51]. The addition of carbon nitride to SiC caused a strong decrease of the PL bands intensity, mainly for the SiC 0.5% g-C_3N_4, and the SiC 1% g-C_3N_4 composites, suggesting that an efficient charge carriers separation occurred on the SiC-low amount of g-C_3N_4 heterostructures [52].

The crystallinity of the as-prepared samples was investigated by XRD (Fig. 7). From the XRD patterns it was possible to note that the diffraction peaks of the synthesized C_3N_4 at 2θ = 12.9° and 27.4°,

Table 1
Optical and textural properties of the examined samples.

Samples	Optical band gap (eV)	BET surface area (m^2/g)	Mean pores diameter (nm)	Pores volume (cm^3/g)
g-C_3N_4	2.85	66.8	8.9	0.24
SiC	2.96	17.4	18.6	0.45
SiC 0,5% g-C_3N_4	2.94	17.9	18.4	0.44
SiC 1% g-C_3N_4	2.95	20.5	17.4	0.43
SiC 2% g-C_3N_4	2.95	22.8	15.9	0.39

correspond to the crystalline planes (100) and (002) respectively, associated to the tetragonal C_3N_4 in the graphitic form [53]. The SiC-based samples showed diffraction peaks at 2θ = 37°, 42°, 61.3°, 67° corresponding to the cubic 3C-SiC (β-SiC) structure and the crystalline planes (111), (200), (220), and (311) respectively [53]. The peaks in the range 2θ = 33–35° were associated to the spontaneous packing fault related to the SiC growth [52]. In the SiC-based samples the peaks related to the carbon nitride are not present probably due to the low amount of g-C_3N_4. Furthermore, comparing the TEM images of the bare SiC (Fig. S4A) and of SiC 1% g-C_3N_4 (chosen at representative sample being the best one for the PET photoreforming, Figs. S4B-C) it is possible verify the interaction between the SiC particles and the g-C_3N_4 sheets.

The surface properties of the as-prepared samples were characterized by XPS (Fig. 8). Fig. 8A shows the high-resolution XP spectrum of the SiC 1% g-C_3N_4 sample (as representative sample) in the C 1s binding energy region. Two evident signals appear at 282.5 and 285.0 eV due to the carbide states and to the adventitious surface carbon, omnipresent on air thermally-threated materials, respectively [54,55]. In the Si 2p binding energy region (Fig. 8B), the two bands at 100.4 and 103.2 eV are due to the Si states of the carbide and to some SiO_x species [54,55], whose formation was also confirmed by the XP spectrum in the O 1s binding energy region (Fig. 8C), with the unique peak at 532.4 eV, in agreement with the presence of SiO_x species [56]. The same signals are present in all the SiC-based materials, including the bare SiC (Figs. S5).

Fig. S6A shows the high-resolution XP spectrum of the bare g-C_3N_4 in the C 1s binding energy region. The two evident signals at 288.2 and 284.7 eV are due to the carbon C—N states of the C_3N_4 and to the adventitious carbon, respectively [57]. Fig. S6B shows the high-resolution XP spectrum of the carbon nitride in the N 1s binding energy region. A strong signal appears at 398.6 eV with a shoulder at higher binding energy (about 401 eV) and even a very low, but sizeable, band at 404.1 eV. The first signal is due to the expected C=N-C and C_3—N states of the g-C_3N_4 while the B.E. value of the shoulder is compatible with the nitrogen of NH_2-C=O and/or positive N^+ states

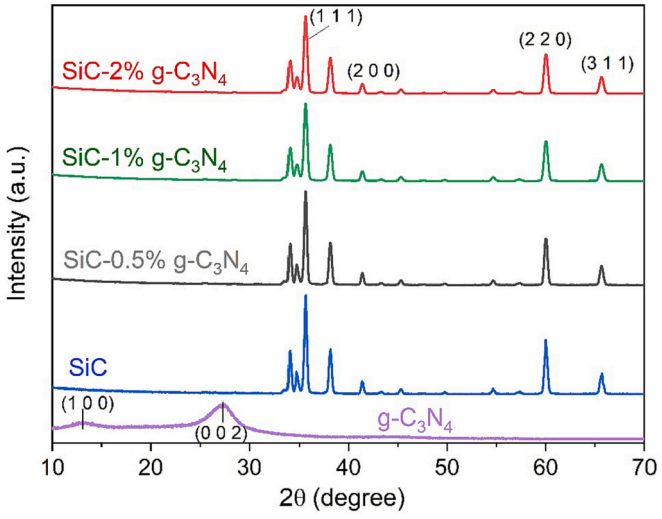

Fig. 7. XRD patterns of the examined samples.

[57,58]. Finally, the small band at 404.1 eV is due to some negligible nitrite/nitrate [59].The signal at 398.6 eV of the carbon nitride is present (with low intensity, due to the low amount added to the SiC) also in the SiC 1% g-C_3N_4 sample (Fig. 8D) and in all SiC-based composites.

In summary, the SiC-g-C_3N_4 composites are promising photocatalysts that allowed to obtain H_2 from plastic-related materials. The presence of SiC is fundamental, due to its chemical stability under the extreme basic conditions of the photoreforming reactions, whereas the addition of small amounts of graphitic carbon nitride allowed to increase the charge carriers separation, as confirmed by the PL spectroscopy. The good interaction between the two components of the composites increased the H_2 evolution compared to the bare SiC and g-C_3N_4 samples. In accordance with the literature [52,53,60], this interaction is basically established by van der Waals interfaces formed during the synthesis of the SiC-g-C_3N_4 composite, where the SiC particles were strewn on the as-formed g-C_3N_4 sheets, as verified by TEM (Fig. S4).

Only a low content of carbon nitride (0.5 or 1 wt%) allowed to increase the performance of the bare SiC. Noteworthy, no substantial variations were detected in the optical band gap of the SiC-g-C_3N_4 composites compared to the bare SiC (2.94–2.96 eV, Table 1). On the basis of these data, bearing in mind the reported bands position of SiC and g-C_3N_4 [52,61] and considering that the samples were prepared with simple physical mixture of commercial SiC powders with urea (precursor of carbon nitride), followed by a thermal treatment, a scheme of the proposed photocatalytic mechanism is shown in the Fig. 9. The SiC particles were deposited on g-C_3N_4 sheets enabling a good interaction between them. Upon solar irradiation, both SiC and g-C_3N_4 were excited and thus electrons (e^-) and holes (h^+) were formed in the conduction (CB) and valence bands (VB) of the two materials, respectively. The electrons moved from the CB of g-C_3N_4 to that of SiC and holes migrated from the VB of SiC to that of g-C_3N_4, promoting a good charge carriers separation. In this way, the holes were able to oxidize water to H^+ and to hydroxyl radicals. These latter species were able to degrade the plastic materials with the formation of byproducts that can promote further photoreforming reactions. The generated H^+ species were reduced by the electrons gathered at the CB of SiC, allowing the H_2 evolution.

The photoreforming of PET led to higher H_2 production rate compared to the bare BPA and this was ascribed to the pretreatment conditions. Indeed, the strong basic environment favoured, in the case of PET, its hydrolysis with the formation of ethylene glycol (as verified by ^{1}H- NMR) which further photoreforming that promoted the H_2 formation. On the contrary the BPA photodegradation was more difficult with a lower hydrogen production. The pH of the reaction was another key parameter, being pH = 13 the best compromise for the optimal interaction among the reactants and the negative charged surface of SiC (Fig. 5B). This pH was also the ideal one for the BPA and PET pretreatments, in accordance with the literature data [62,63]. Neutral, acidic, or less basic solutions (pH < 13) did not allow to obtain sufficient H_2 production both for PET and BPA photoreforming.

Although it is not easy to carry out an accurate comparison with the literature data, due to the different experimental set-ups employed by the various research groups and due to the novelty of the plastic photorefoming reaction, it is noteworthy that the here reported performance of the SiC-1%g-C_3N_4 composite in the simulated solar light driven-PET photoreforming (18 $\mu molH_2/g_{cat}\bullet h$) was better than that of some TiO_2-based samples or carbon nitride porous microtube (CN_xPM)

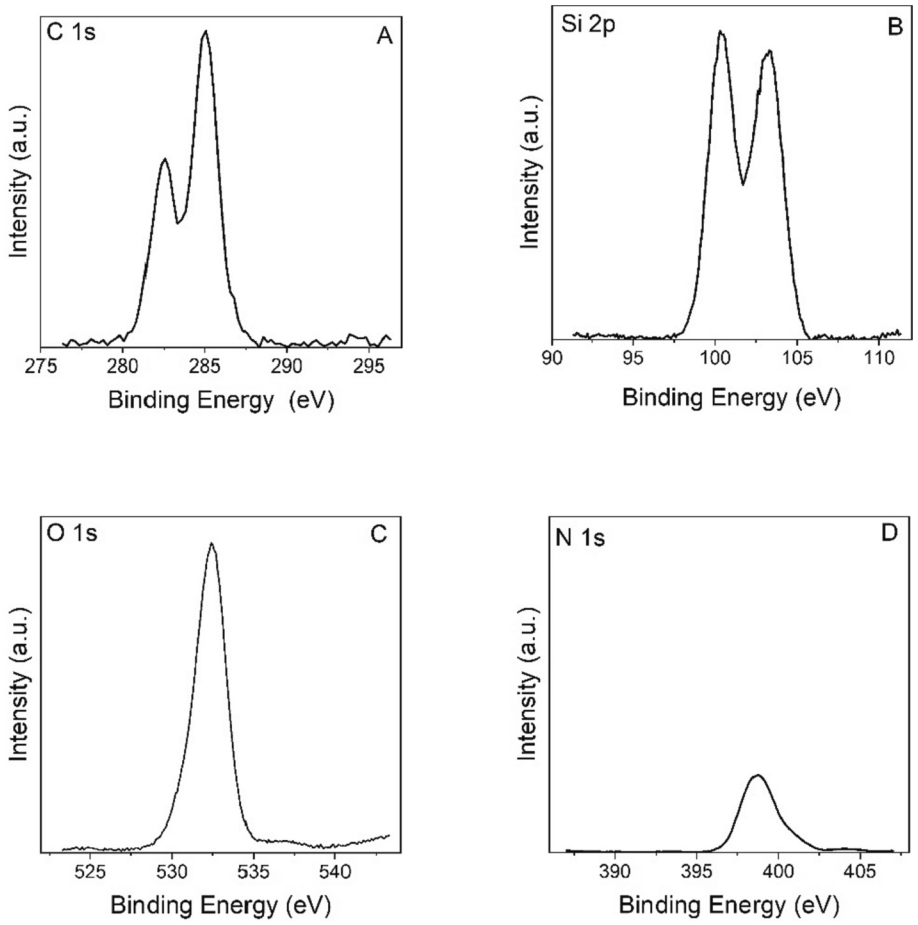

Fig. 8. Al Kα excited XPS of the SiC-1%g-C_3N_4 sample in the (A) C 1s (B) Si 2p, (C) O 1s and (D) N 1s binding energy regions.

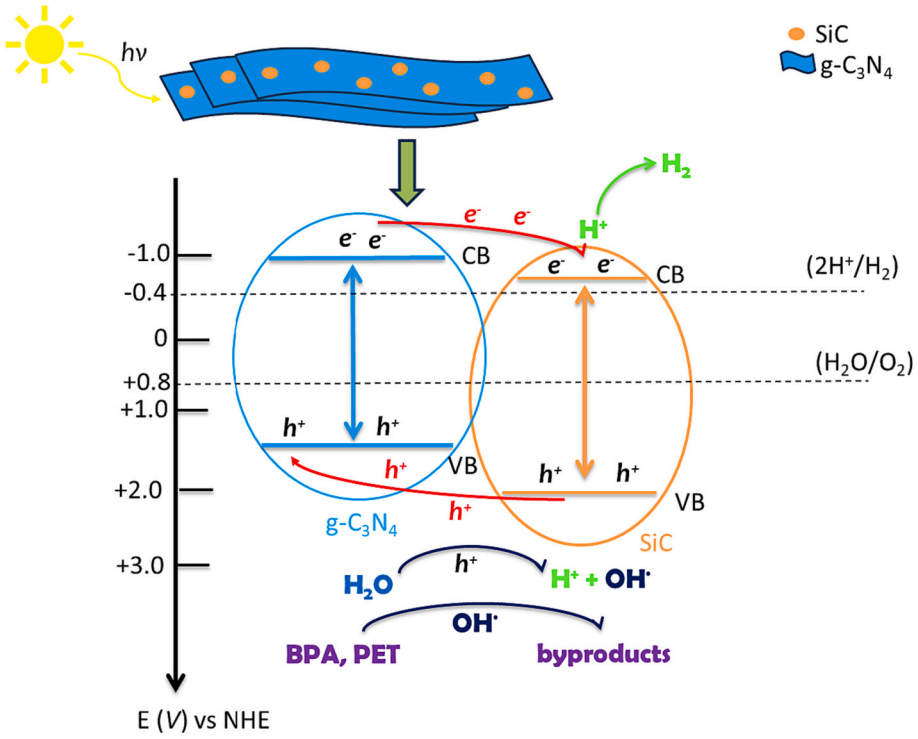

Fig. 9. Schematic illustration of the proposed photocatalytic mechanism.

Table 2
Comparison among different photocatalysts employed for the PET photoreforming.

Samples	PET pretreatment	Irradiation source	H_2 production rate ($\mu molH_2/g_{cat}•h$)	Ref.
SiC 1 wt% g-C_3N_4	NaOH solution 10 M at 40° C	solar lamp 10.7 mW/cm^2	18.1	this work
TiO_2 5 wt% Au	KOH solution 10 M at 40° C	high pressure UV mercury vapor lamp 60 mW/cm^2	3.0	[64]
TiO_2-Ni2P	KOH solution 10 M at 40 °C	simulated solar light AM 1.5G, 100 mW/cm^2	13.8	[9]
CN_xPM	/	300 W Xenon arc lamp equipped with a cut-off filter ($\lambda > 420$ nm)	9.4	[65]
CN_x-Ni2P	KOH solution 10 M at 40 °C	simulated solar light AM 1.5G, 100 mW/cm^2	33.1	[9]
$Cd_{0.5}$ $Zn_{0.5}S$	NaOH solution 10 M at 35 °C	300 W xenon lamp with a cut-off filter ($\lambda > 420$ nm)	74.4	[66]

photocatalysts (Table 2), but worse with respect to CN_x-Ni2P or $Cd_{0.5}$ $Zn_{0.5}S$ samples (Table 2).

Reasonably, we expected that the H_2 production can be further improved by tailoring the interaction and therefore the heterostructures between SiC and g-C_3N_4 or by preparing other more efficient photocatalyst composites. This work, however, shows as it is possible to transform an environmental problem, as the water pollution by plastic materials, into a sustainable opportunity to produce hydrogen and/or high-added value products from pollutants. This is a relevant and recent topic with several fascinating opportunities as the design of the chemico-physical properties of the employed photocatalysts on the basis of the plastic materials used as organic scavengers. A recent review of *Ashraf* et al. [34] examined the performance of various photocatalysts in the photoreforming of other plastic materials as polyethylene (PE), polystyrene (PS), polyvinyl chloride (PVC), polyurethane (PU) and polylactic acid (PLA), discussing also the byproducts selectivity and the pretreatment conditions. Recently, hybrid catalysis, as the photothermocatalysis, was applied to accelerate the degradation of biodegradable plastics as the PLA with the contextual H_2 production [67], and chemoenzymatic approaches were used to produce H_2 from the reforming of polyester films and nanoplastics [68].These new data and research, combined with the new technologies related to the photocatalytic degradation of plastics [69,70] can help to find more efficient and performing solutions to the plastic waste disposal and upcycling.

4. Conclusions

The performance of the SiC-g-C_3N_4 composites, prepared with an easy procedure, was investigated in the solar PET and the BPA photoreforming. The addition of small amounts of carbon nitride to SiC resulted in a good SiC/g-C_3N_4 interaction with a negative superficial charge which boosted the H_2 evolution from both reactions. The PET substrate led to the higher H_2 production rate, and this was related to the formation of intermediates (among all ethylene glycol) which further promoted the photoreforming. The strongly basic pH (13) was essential to favour both the plastic materials pretreatment and the interaction between the reactants and the surface of the SiC-g-C_3N_4 composites. Finally, urea was the best carbon nitride precursor for the formation of SiC-g-C_3N_4 composites active for these reactions. The results obtained in this work pave the way to new photocatalysts for the plastic materials photoreforming, enlarging the future environmental perspectives in which the wastes or the pollutants can be considered new raw materials to obtain H_2 preserving, contextually, the water by the emerging contaminants.

CRediT authorship contribution statement

Maria Teresa Armeli Iapichino: Writing – original draft, Methodology, Investigation, Data curation, Conceptualization. **Roberto Fiorenza:** Writing – review & editing, Writing – original draft, Validation, Supervision, Investigation, Conceptualization. **Vincenzo Patamia:** Investigation. **Giuseppe Floresta:** Investigation. **Antonino Gulino:** Investigation. **Marcello Condorelli:** Investigation. **Giuliana Impellizzeri:** Investigation. **Giuseppe Compagnini:** Visualization, Funding acquisition. **Salvatore Sciré:** Writing – review & editing, Visualization, Supervision, Resources, Funding acquisition.

Declaration of competing interest

The authors declare that they have no known competing financial interests or personal relationships that could have appeared to influence the work reported in this paper.

Data availability

Data will be made available on request.

Acknowledgements

The authors thank the research group of prof. F.J. Urbano (University of Cordoba) and Dr. Stefano Andrea Balsamo for the TEM measurements and prof. G. Malandrino (University of Catania) and the Bio-nanotech Research and Innovation Tower (BRIT) laboratory of the University of Catania (Grant no. PONa3_00136 financed by the MIUR) for the Smartlab diffractometer facility. The BRIT was also thanked for the XPS measurements. The PIACERI 2020-2022 project of the University of Catania was acknowledged for the support. SalvatoreScirè thanks the European Union (NextGeneration EU) MUR-PNRR project SAMOTHRACE (ECS00000022).

Appendix A. Supplementary data

Supplementary data to this article can be found online at https://doi.org/10.1016/j.catcom.2024.106850.

References

[1] M. Rumayor, J. Corredor, M.J. Rivero, I. Ortiz, Prospective life cycle assessment of hydrogen production by waste photoreforming, J. Clean. Prod. 336 (2022) 130430, https://doi.org/10.1016/j.jclepro.2022.130430.
[2] F.J. López-Tenllado, R. Estévez, J. Hidalgo-Carrillo, S. López-Fernández, F. J. Urbano, A. Marinas, Hydrogen photo-production from glycerol on platinum, gold and silver-modified TiO_2_USY62 catalysts, Catal. Today. 390–391 (2022) 92–98, https://doi.org/10.1016/j.cattod.2021.11.043.
[3] R. Singh, S. Dutta, A review on H2 production through photocatalytic reactions using TiO_2/TiO_2-assisted catalysts, Fuel. 220 (2018) 607–620, https://doi.org/10.1016/j.fuel.2018.02.068.
[4] K.C. Christoforidis, P. Fornasiero, Photocatalytic hydrogen production: a rift into the future energy supply, ChemCatChem. 9 (2017) 1523–1544, https://doi.org/10.1002/cctc.201601659.
[5] S.A. Balsamo, E. La Greca, M. Calà Pizzapilo, S. Sciré, R. Fiorenza, CeO_2-rGO composites for photocatalytic H_2 evolution by glycerol Photoreforming, Materials 16 (2023) 747, https://doi.org/10.3390/ma16020747.
[6] D. Banerjee, N. Kushwaha, N.P. Shetti, T.M. Aminabhavi, E. Ahmad, Green hydrogen production via photo-reforming of bio-renewable resources, Renew. Sustain. Energy Rev. 167 (2022) 112827, https://doi.org/10.1016/j.rser.2022.112827.
[7] S.A. Balsamo, R. Fiorenza, M.T.A. Iapichino, F.J. Lopez-Tenllado, F.J. Urbano, S. Sciré, H_2 production through glycerol photoreforming using one-pot prepared TiO_2-rGO-au photocatalysts, Mol. Catal. 547 (2023) 113346, https://doi.org/10.1016/j.mcat.2023.113346.
[8] S. Gazzotti, B. De Felice, M.A. Ortenzi, M. Parolini, Approaches for management and valorization of non-homogeneous, non-recyclable plastic waste, Int. J. Environ. Res. Public Health 19 (2022) 10088, https://doi.org/10.3390/ijerph191610088.

[9] T. Uekert, H. Kasap, E. Reisner, Photoreforming of nonrecyclable plastic waste over a carbon nitride/nickel phosphide catalyst, J. Am. Chem. Soc. 141 (2019) 15201–15210, https://doi.org/10.1021/jacs.9b06872.

[10] E.M. Malannata, L. Spitaleri, A. Gulino, S.A. Balsamo, S. Scirè, R. Fiorenza, Removal of phthalates from water by unconventional La-based/WO_3 Photocatalysts, Eur. J. Inorg. Chem. (2022) e202200183, https://doi.org/10.1002/ejic.202200183.

[11] J. Liu, X. Li, C. Han, M. Liu, X. Li, J. Sun, C. Shao, Hetero-Janus nanofibers as an ideal framework for promoting water-pollutant Photoreforming hydrogen evolution, Energy Environ. Mater. 6 (2023) e12404, https://doi.org/10.1002/eem2.12404.

[12] L. Wang, X. Jiang, Y. Liu, Degradation of bisphenol a and formation of hydrogen peroxide induced by glow discharge plasma in aqueous solutions, J. Hazard. Mater. 154 (2008) 1106–1114, https://doi.org/10.1016/j.jhazmat.2007.11.016.

[13] X. Gong, F. Tong, F. Ma, Y. Zhang, P. Zhou, Z. Wang, Y. Liu, P. Wang, H. Cheng, Y. Dai, Z. Zheng, B. Huang, Photoreforming of plastic waste poly (ethylene terephthalate) via in-situ derived CN-CNTs-NiMo hybrids, Appl. Catal. Environ. 307 (2022) 121143, https://doi.org/10.1016/j.apcatb.2022.121143.

[14] C.A. Walenta, M. Tschurl, U. Heiz, Introducing catalysis in photocatalysis: what can be understood from surface science studies of alcohol photoreforming on TiO_2, J. Phys. Condens. Matter 31 (2019) 473002, https://doi.org/10.1088/1361-648X/ab351a.

[15] E. Lewicka, K. Guzik, K. Galos, On the possibilities of critical raw materials production from the EU's primary sources, Resources 10 (2021) 50, https://doi.org/10.3390/resources10050050.

[16] S.R. Kulkarni, V.K. Velisoju, F. Tavares, A. Dikhtiarenko, J. Gascon, P. Castaño, Silicon carbide in catalysis: from inert bed filler to catalytic support and multifunctional material, Catal. Rev. 65 (2023) 174–237, https://doi.org/10.1080/01614940.2022.2025670.

[17] G. Xi, Y. Liu, X. Liu, X. Wang, Y. Qian, Mg-catalyzed autoclave synthesis of aligned silicon carbide nanostructures, J. Phys. Chem. B 110 (2006) 14172–14178, https://doi.org/10.1021/jp0617468.

[18] H. Gao, S. Yan, J. Wang, Y.A. Huang, P. Wang, Z. Li, Z. Zou, Towards efficient solar hydrogen production by intercalated carbon nitride photocatalyst, Phys. Chem. Chem. Phys. 15 (2013) 18077, https://doi.org/10.1039/c3cp53774a.

[19] W. Wan, S. Yu, F. Dong, Q. Zhang, Y. Zhou, Efficient C_3N_4/graphene oxide macroscopic aerogel visible-light photocatalyst, J. Mater. Chem. A 4 (2016) 7823–7829, https://doi.org/10.1039/C6TA01804A.

[20] C. Prasad, H. Tang, Q. Liu, I. Bahadur, S. Karlapudi, Y. Jiang, A latest overview on photocatalytic application of g-C_3N_4 based nanostructured materials for hydrogen production, Int. J. Hydrogen Energy 45 (2020) 337–379, https://doi.org/10.1016/j.ijhydene.2019.07.070.

[21] B. Zhu, B. Cheng, J. Fan, W. Ho, J. Yu, G-C_3N_4 -based 2D/2D composite heterojunction Photocatalyst, Small Struct. 2 (2021), https://doi.org/10.1002/sstr.202100086.

[22] S. Riaz, S.-J. Park, Carbon quantum dots-embedded graphitic carbon nitride nanotubes for enhancing the power conversion efficiency of sensitized solar cells, Mater. Today Chem. 24 (2022) 100763, https://doi.org/10.1016/j.mtchem.2021.100763.

[23] P. Makuła, M. Pacia, W. Macyk, How to correctly determine the band gap energy of modified semiconductor Photocatalysts based on UV–vis spectra, J. Phys. Chem. Lett. 9 (2018) 6814–6817, https://doi.org/10.1021/acs.jpclett.8b02892.

[24] G. Greczynski, L. Hultman, Compromising science by ignorant instrument calibration—need to revisit half a century of published XPS data, Angew. Chemie Int. Ed. 59 (2020) 5002–5006, https://doi.org/10.1002/anie.201916000.

[25] A. Gulino, Structural and electronic characterization of self-assembled molecular nanoarchitectures by X-ray photoelectron spectroscopy, Anal. Bioanal. Chem. 405 (2013) 1479–1495, https://doi.org/10.1007/s00216-012-6394-8.

[26] R. Fiorenza, S.A. Balsamo, M. Condorelli, L. D'Urso, G. Compagnini, S. Scirè, Solar photocatalytic H_2 production over CeO_2-based catalysts: influence of chemical and structural modifications, Catal. Today 380 (2021) 187–198, https://doi.org/10.1016/j.cattod.2021.02.003.

[27] Y. Li, S. Wan, C. Lin, Y. Gao, Y. Lu, L. Wang, K. Zhang, Engineering of 2D/2D MoS_2 /$Cd_xZn_{1-x}S$ Photocatalyst for solar H_2 evolution coupled with degradation of plastic in alkaline solution, Sol. RRL. 5 (2021), https://doi.org/10.1002/solr.202000427.

[28] I.M. Figueiredo, N.R. Pereira, P. Efraim, N.H.P. García, N.R. Rodrigues, A. Marsaioli, A.J. Marsaioli, 1 H NMR, a rapid method to monitor organic acids during Cupuassu (Theobroma grandiflorum Spreng) processing, J. Agric. Food Chem. 54 (2006) 4102–4106, https://doi.org/10.1021/jf0525176.

[29] J. Wang, Q. Zhou, Y. Shen, X. Chen, S. Liu, Y. Zhang, Carbon nitride co-catalyst activation using N-doped carbon with enhanced photocatalytic H_2 evolution, Langmuir. 35 (2019) 12366–12373, https://doi.org/10.1021/acs.langmuir.9b01796.

[30] K. Qi, S. Liu, A. Zada, Graphitic carbon nitride, a polymer photocatalyst, J. Taiwan Inst. Chem. Eng. 109 (2020) 111–123, https://doi.org/10.1016/j.jtice.2020.02.012.

[31] P. Shandilya, A. Guleria, B. Fang, A magnetically recyclable dual step-scheme Bi_2WO_6/Fe_2O_3/WO_3 heterojunction for photodegradation of bisphenol-a from aqueous solution, J. Environ. Chem. Eng. 9 (2021) 106461, https://doi.org/10.1016/j.jece.2021.106461.

[32] N. Watanabe, S. Horikoshi, H. Kawabe, Y. Sugie, J. Zhao, H. Hidaka, Photodegradation mechanism for bisphenol a at the TiO_2/H_2O interfaces, Chemosphere. 52 (2003) 851–859, https://doi.org/10.1016/S0045-6535(02)00837-8.

[33] D. Gunawan, C.Y. Toe, P. Kumar, J. Scott, R. Amal, Synergistic Cyanamide functionalization and charge-induced activation of nickel/carbon nitride for enhanced selective Photoreforming of ethanol, ACS Appl. Mater. Interfaces 13 (2021) 49916–49926, https://doi.org/10.1021/acsami.1c14195.

[34] M. Ashraf, N. Ullah, I. Khan, W. Tremel, S. Ahmad, M.N. Tahir, Photoreforming of waste polymers for sustainable hydrogen fuel and chemicals feedstock: waste to energy, Chem. Rev. 123 (2023) 4443–4509, https://doi.org/10.1021/acs.chemrev.2c00602.

[35] T. Uekert, M.F. Kuehnel, D.W. Wakerley, E. Reisner, Plastic waste as a feedstock for solar-driven H_2 generation, Energ. Environ. Sci. 11 (2018) 2853–2857, https://doi.org/10.1039/C8EE01408F.

[36] B. Cao, S. Wan, Y. Wang, H. Guo, M. Ou, Q. Zhong, Highly-efficient visible-light-driven photocatalytic H_2 evolution integrated with microplastic degradation over MXene/$ZnxCd_{1-x}S$ photocatalyst, J. Colloid Interface Sci. 605 (2022) 311–319, https://doi.org/10.1016/j.jcis.2021.07.113.

[37] Q. Liang, B. Shao, S. Tong, Z. Liu, L. Tang, Y. Liu, M. Cheng, Q. He, T. Wu, Y. Pan, J. Huang, Z. Peng, Recent advances of melamine self-assembled graphitic carbon nitride-based materials: design, synthesis and application in energy and environment, Chem. Eng. J. 405 (2021) 126951, https://doi.org/10.1016/j.cej.2020.126951.

[38] H.-S. Zhai, L. Cao, X.-H. Xia, Synthesis of graphitic carbon nitride through pyrolysis of melamine and its electrocatalysis for oxygen reduction reaction, Chinese Chem. Lett. 24 (2013) 103–106, https://doi.org/10.1016/j.cclet.2013.01.030.

[39] R.C. Dante, P. Martín-Ramos, A. Correa-Guimaraes, J. Martín-Gil, Synthesis of graphitic carbon nitride by reaction of melamine and uric acid, Mater. Chem. Phys. 130 (2011) 1094–1102, https://doi.org/10.1016/j.matchemphys.2011.08.041.

[40] A. Sudhaik, P. Raizada, P. Shandilya, D.-Y. Jeong, J.-H. Lim, P. Singh, Review on fabrication of graphitic carbon nitride based efficient nanocomposites for photodegradation of aqueous phase organic pollutants, J. Ind. Eng. Chem. 67 (2018) 28–51, https://doi.org/10.1016/j.jiec.2018.07.007.

[41] S. Cao, J. Low, J. Yu, M. Jaroniec, Polymeric Photocatalysts based on graphitic carbon nitride, Adv. Mater. 27 (2015) 2150–2176, https://doi.org/10.1002/adma.201500033.

[42] Q. Dong, Z. Chen, B. Zhao, Y. Zhang, Z. Lu, X. Wang, J. Li, W. Chen, In situ fabrication of niobium pentoxide/graphitic carbon nitride type-II heterojunctions for enhanced photocatalytic hydrogen evolution reaction, J. Colloid Interface Sci. 608 (2022) 1951–1959, https://doi.org/10.1016/j.jcis.2021.10.161.

[43] Y. Hong, E. Liu, J. Shi, X. Lin, L. Sheng, M. Zhang, L. Wang, J. Chen, A direct one-step synthesis of ultrathin g-C_3N_4 nanosheets from thiourea for boosting solar photocatalytic H_2 evolution, Int. J. Hydrogen Energy 44 (2019) 7194–7204, https://doi.org/10.1016/j.ijhydene.2019.01.274.

[44] Y.-P. Yuan, L.-S. Yin, S.-W. Cao, L.-N. Gu, G.-S. Xu, P. Du, H. Chai, Y.-S. Liao, C. Xue, Microwave-assisted heating synthesis: a general and rapid strategy for large-scale production of highly crystalline g-C_3N_4 with enhanced photocatalytic H_2 production, Green Chem. 16 (2014) 4663–4668, https://doi.org/10.1039/C4GC01517G.

[45] F. Dong, Z. Wang, Y. Sun, W.-K. Ho, H. Zhang, Engineering the nanoarchitecture and texture of polymeric carbon nitride semiconductor for enhanced visible light photocatalytic activity, J. Colloid Interface Sci. 401 (2013) 70–79, https://doi.org/10.1016/j.jcis.2013.03.034.

[46] H. Yan, Soft-templating synthesis of mesoporous graphitic carbon nitride with enhanced photocatalytic H_2 evolution under visible light, Chem. Commun. 48 (2012) 3430, https://doi.org/10.1039/c2cc00001f.

[47] B. Wang, Y. Wang, Y. Lei, N. Wu, Y. Gou, C. Han, S. Xie, D. Fang, Mesoporous silicon carbide nanofibers with in situ embedded carbon for co-catalyst free photocatalytic hydrogen production, Nano Res. 9 (2016) 886–898, https://doi.org/10.1007/s12274-015-0971-z.

[48] S. Chen, Y. Hu, X. Jiang, S. Meng, X. Fu, Fabrication and characterization of novel Z-scheme photocatalyst WO_3/g-C_3N_4 with high efficient visible light photocatalytic activity, Mater. Chem. Phys. 149–150 (2015) 512–521, https://doi.org/10.1016/j.matchemphys.2014.11.001.

[49] H. Huang, X. Li, J. Wang, F. Dong, P.K. Chu, T. Zhang, Y. Zhang, Anionic group self-doping as a promising strategy: band-gap engineering and multi-functional applications of high-performance CO_3^{2-}-DopedBi_2O_2 CO_3, ACS Catal. 5 (2015) 4094–4103, https://doi.org/10.1021/acscatal.5b00444.

[50] N. Tian, Y. Zhang, X. Li, K. Xiao, X. Du, F. Dong, G.I.N. Waterhouse, T. Zhang, H. Huang, Precursor-reforming protocol to 3D mesoporous g-C_3N_4 established by ultrathin self-doped nanosheets for superior hydrogen evolution, Nano Energy 38 (2017) 72–81, https://doi.org/10.1016/j.nanoen.2017.05.038.

[51] K.-H. Lee, S.-K. Lee, K.-S. Jeon, Photoluminescent properties of silicon carbide and porous silicon carbide after annealing, Appl. Surf. Sci. 255 (2009) 4414–4420, https://doi.org/10.1016/j.apsusc.2008.11.047.

[52] F. Chang, J. Zheng, X. Wang, Q. Xu, B. Deng, X. Hu, X. Liu, Heterojuncted non-metal binary composites silicon carbide/g-C_3N_4 with enhanced photocatalytic performance, Mater. Sci. Semicond. Process. 75 (2018) 183–192, https://doi.org/10.1016/j.mssp.2017.11.043.

[53] U. Baig, A. Khan, M.A. Gondal, M.A. Dastageer, S. Akhtar, Single-step synthesis of silicon carbide anchored graphitic carbon nitride nanocomposite photo-catalyst for efficient photoelectrochemical water splitting under visible-light irradiation, Colloids Surfaces A Physicochem. Eng. Asp. 611 (2021) 125886, https://doi.org/10.1016/j.colsurfa.2020.125886.

[54] M.D. Pirnaci, L. Spitaleri, D. Tenaglia, F. Perricelli, M.E. Fragalà, C. Bongiorno, A. Gulino, Systematic characterization of plasma-etched trenches on 4H-SiC wafers, ACS Omega 6 (2021) 20667–20675, https://doi.org/10.1021/acsomega.1c02905.

[55] G. Mishra, K.M. Parida, S.K. Singh, Facile fabrication of S-TiO_2 /β-SiC nanocomposite Photocatalyst for hydrogen evolution under visible light irradiation, ACS Sustain. Chem. Eng. 3 (2015) 245–253, https://doi.org/10.1021/sc500570k.
[56] A. Gulino, G.G. Condorelli, P. Mineo, I. Fragalà, An x-ray photoelectron spectra and atomic force microscopy characterization of silica substrates engineered with a covalently assembled siloxane monolayer, Nanotechnology. 16 (2005) 2170–2175, https://doi.org/10.1088/0957-4484/16/10/033.
[57] M.H. Vu, C.C. Nguyen, T. Do, Graphitic carbon nitride (g-C_3N_4) nanosheets as a multipurpose material for detection of amines and solar-driven hydrogen production, ChemPhotoChem. 5 (2021) 466–475, https://doi.org/10.1002/cptc.202000265.
[58] L. Motiei, M. Altman, T. Gupta, F. Lupo, A. Gulino, G. Evmenenko, P. Dutta, M. E. van der Boom, Self-propagating assembly of a molecular-based multilayer, J. Am. Chem. Soc. 130 (2008) 8913–8915, https://doi.org/10.1021/ja802470g.
[59] D. Briggs, J.T. Grant, In Surface Analysis by Auger and X-Ray Photoelectron Spectroscopy, IM Publications, Chichester, UK, and Surface Spectra Ltd., Manchester, UK, 2003.
[60] Z. Wu, Y. Li, X. Li, E. Feng, L.A. Cao, Z. Li, X. Wang, P. Jiang, D. Wang, Acid protonation promoted different crystal phase structure silicon carbide-based carbon nitride composites to enhance the photocatalytic degradation of dye wastewater, RSC Adv. 13 (2023) 35672–35682, https://doi.org/10.1039/d3ra06438g.
[61] Z. Du, P. Sun, K. Wu, X. Zheng, X. Zhang, J. Huang, D. Sun, Y. Zheng, Q. Li, G-C3N4-SiC-Pt for enhanced photocatalytic H_2 production from water under visible light irradiation, Energ. Technol. 7 (2019) 1–10, https://doi.org/10.1002/ente.201900017.
[62] T. Uekert, M.A. Bajada, T. Schubert, C.M. Pichler, E. Reisner, Scalable Photocatalyst panels for Photoreforming of plastic, biomass and mixed waste in flow, ChemSusChem. 14 (2021) 4190–4197, https://doi.org/10.1002/cssc.202002580.
[63] D.T. Li, H. Yu, Y. Huang, Facile H_2PdCl^{4-}induced photoreforming of insoluble PET waste for C1-C3 compound production, Front. Chem. 11 (2023), https://doi.org/10.3389/fchem.2023.1265556.
[64] E.M.N.T. Edirisooriya, P.S. Senanayake, H.B. Wang, M.R. Talipov, P. Xu, H. Wang, Photo-reforming and degradation of waste plastics under UV and visible light for H_2 production using nanocomposite photocatalysts, J. Environ. Chem. Eng. 11 (2023) 109580, https://doi.org/10.1016/j.jece.2023.109580.
[65] S. Guo, Y. Huang, D. Li, Z. Xie, Y. Jia, X. Wu, D. Xu, W. Shi, Visible-light-driven photoreforming of poly(ethylene terephthalate) plastics via carbon nitride porous microtubes, Chem. Commun. 59 (2023) 7791–7794, https://doi.org/10.1039/D3CC02012F.
[66] R. Li, F. Wang, F. Lv, P. Wang, X. Guo, J. Feng, D. Li, Y. Chen, Simultaneous hydrogen production and conversion of plastic wastes into valued chemicals over a Z-scheme photocatalyst, Int. J. Hydrogen Energy 51 (2024) 406–414, https://doi.org/10.1016/j.ijhydene.2023.10.069.
[67] D. Jiang, H. Yuan, Z. Liu, Y. Chen, Y. Li, X. Zhang, G. Xue, H. Liu, X. Liu, L. Zhao, W. Zhou, Defect-anchored single-atom-layer Pt clusters on TiO2−x/Ti for efficient hydrogen evolution via photothermal reforming plastics, Appl. Catal. Environ. 339 (2023) 123081, https://doi.org/10.1016/j.apcatb.2023.123081.
[68] S. Bhattacharjee, C. Guo, E. Lam, J.M. Holstein, M. Rangel Pereira, C.M. Pichler, C. Pornrungroj, M. Rahaman, T. Uekert, F. Hollfelder, E. Reisner, Chemoenzymatic Photoreforming: a sustainable approach for solar fuel generation from plastic feedstocks, J. Am. Chem. Soc. 145 (2023) 20355–20364, https://doi.org/10.1021/jacs.3c05486.
[69] S.H. Paiman, S.F. Md Noor, N. Ngadi, A.H. Nordin, N. Abdullah, Insight into photocatalysis technology as a promising approach to tackle microplastics pollution through degradation and upcycling, Chem. Eng. J. 467 (2023) 143534, https://doi.org/10.1016/j.cej.2023.143534.
[70] A.M. Díez, N. Licciardello, Y.V. Kolen'ko, Photocatalytic processes as a potential solution for plastic waste management, Polym. Degrad. Stab. 215 (2023) 110459, https://doi.org/10.1016/j.polymdegradstab.2023.110459.